Hindawi
Adsorption Science & Technology
Volume 2021, Article ID 4150073, 18 pages
https://doi.org/10.1155/2021/4150073

Research Article

Preparation of Magnetic Composite Polyaniline/Fe_3O_4–Hydrotalcite and Performance in Removal of Methyl Orange

Thi Tuong An Tran,[1] Huynh Thanh Linh Duong,[2] Thi Thuy Phuong Pham,[2] Tri Nguyen,[2] Thi Dung Nguyen,[2] and Boi An Tran[2]

[1]*Ho Chi Minh City University of Technology, 268 Ly Thuong Kiet, Ward 14, District 10, Ho Chi Minh City, Vietnam*
[2]*Institute of Chemical Technology, Vietnam Academy of Science and Technology, 1A TL29, Thanh Loc Ward, District 12, Ho Chi Minh City, Vietnam*

Correspondence should be addressed to Boi An Tran; tranboian@gmail.com

Received 29 July 2021; Revised 26 August 2021; Accepted 29 October 2021; Published 1 December 2021

Academic Editor: S Rangabhashiyam

Magnetic composite fabricated from polyaniline and Fe_3O_4-hydrotalcite (Pan/MHT) was successfully applicated for removal of methyl orange (MO) from wastewater. The structure and properties of Pan/MHT were characterized by Fourier-transform infrared spectroscopy, scanning electron microscopy, X-ray diffraction, vibrating sample magnetometer, and Brunauer-Emmett-Teller adsorption isotherm. Adsorption kinetic results indicated that the adsorption process followed pseudosecond-order kinetic model ($R^2 = 0.999$), MO adsorption onto Pan/MHT was well described by Freundlich isotherm ($R^2 = 0.994$), and the MO adsorption capacity of 2 Pan/MHT obtained the highest with $Q_e = 156.25$ mg/g. Batch adsorption experiments were carried out using magnetic composite with the effects of initial MO concentration, solution pH, and adsorbent dosage. The results revealed that the magnetic Pan/MHT exhibited efficient adsorption of MO in the aqueous solution as a result of the affinity for organic dyes, microporous structure, and suitable surface area for adsorption (15,460 m^2/g). The superparamagnetic behavior of Pan/MHT (with$H_c = 18.56$ Oe, $M_s = 23.38 \times 10^{-3}$ emu/g, and$M_r = 0.91 \times 10^{-3}$ emu/g) helps that it could be separated from the solution and performs as an economical and alternative adsorbent to removal and degrade azo dye from wastewater. Pan/MHT was also investigated to reuse after desorption of MO in 0.1 M HCl, and the results show that 2 Pan/MHT can be reused for 4 cycles with $Q_e = 79.66$ mg/g.

1. Introduction

Dyes are widely used in many fields, such as textile, cosmetic, pigment, paper industry, dyeing, or tanning industry. In particular, textile industry wastewater contains a lot of dyes with large molecule structure including the azo group which is sustainable and difficult to decompose [1]. The presence of organic dyes is a main cause of environmental pollution problems because they are nonbiodegradable; so, an effective method is necessary to remove them from wastewater sources. It is estimated that 10-15% lost in the effluent during the dyeing process [2]. If they are not promptly treated strictly before releasing to the environment, they can destroy the ecosystem of aquatic organisms and threaten the self-cleaning capacity of the receiving source and the human life.

In recent years, there are many applications for treatment such as membrane filtration, redox, electrochemical, adsorption, and biological methods. Among them, adsorption is the popular method because of its efficiency and economy. The adsorbents which were widely used to remove azo dyes are either inorganic such as activated carbon [3–6], hydrotalcite [7–10], diatomite [11–15] and bentonite [16–19], or organic such as chitosan, alginate, polysaccharide, and polymer materials [20–31] and also hybrid and composite material [32–39]. However, the most challenge for the above adsorbents is the low adsorption capacity and efficiency. Therefore, it is necessary to research and develop new material with good adsorption capacity to treat water contaminated with organic dyes to meet economic efficiency and save costs.

Hydrotalcite (HT) with the general formula is $[M^{2+}_{1-x}M^{3+}_{x}(OH)_2]^{x+}[(A^{n-})_{x/y}.mH_2O]^{x-}$ (M^{2+}: Mg, Zn, Ca, Fe, Ni…; M^{3+}: Al, Cr, Fe…, and A^{n-}: SO_4^{2-}, CO_3^{2-}, F^-, Cl^-, organic anions, or high molecular weight polymers). HTs are interested in using to remove many dyes including MO, amaranth (Am), diamine green B (DGB) and brilliant green (BG), and acid orange (AO) by surface adsorption, interlayer anion exchange, restructuration of calcined HT, and anion exchange [40–42].

Although both polyaniline (Pan) and HT have high adsorption capacity and have been widely used in water treatment. The most important problem is the ability to recover and reuse them. Filtration is an easy method and is widely used but it's not so effective and fast as using the magnetic field. When combined with a magnetic particle Fe_3O_4, the composite or hybrid from HT will have a magnetic property. As a result, the composite produces a constant suspension in an aqueous solution and is immediately separated from the external environment. On the other hand, modification of hydrotalcite including investigation of magnetic Fe_3O_4/HT nanocomposites (MHT) may have great potential for photocatalysis and environmental remediation [43].

As a conductive polymer, polyaniline (Pan) meets the requirements for environmental treatment applications as both an adsorbent and a photo catalyst according to the following characteristics: high adsorption area, flexible bandgap, and steady−state of activation [44]. Pan nanofiber is an effective adsorbent in studying the removal of methyl orange (MO) and black [45, 46]. Pan is also fabricated as a nanotube and nanoparticle, and they all have high efficiency for removal of MO and crystal violet as well as methylene blue [38, 47–51]. Pan nanoparticles give the highest adsorption capacity due to their high surface area of 1083 m^2/g. Besides, it was used as an efficient adsorbent to remove for crystal violet, and methyl orange with the maximum adsorption capacity reaching 245 and 220 mg/g, respectively. In addition, Pan acts as a photo catalyst thanks to its electrical conductivity to increase protonation. Oxidation reactions occur on the catalyst surface, decomposition of the pigment produces intermediate compounds, and the final products are CO_2, SO_4^{2-}, NO_3^-, and NH_4^+. Therefore, the fast charge generation and slow charge recombination lead to enhanced photo catalytic activity.

In summary, both Pan and MHT have high efficiency in the removal of azo dye. However, studies on the adsorption applications of Pan are limited because Pan has a low surface area resulting in low adsorption efficiency. Therefore, many researches are carried out to composing Pan particles with other materials to enhance the adsorption capacity by various synthesis methods. Another way, many reports have shown that MHT material has been suitable for an adsorbent. So, the combination of Pan and MHT to create a Pan/MHT hybrid or composite material has great potential, and it is still not widely exploited for adsorption, especially in wastewater treatment to adsorp dyes (MO, Congo red, ...).

The structure of the hydroxide porous layer and the ability to exchange ions in MHT combined with Pan will give good capacitive properties and high environmental sustainability, because of the special structure that induces ion exchange, restructuration, and the large surface area, so that Pan/MHT can "trap" the MO dye molecules into its structure, recover MO molecules, and remove them from wastewater. In addition, by the restructuring ability, the Pan/MHT material can be desorped for reuse, easily recovered by magnets, saving costs.

For the above advantages of Pan/MHT composite, in this paper, we synthesized Pan/MHT composite with various mass ratios of $m_{Pan}/m_{MHT} = 0.5$, 1, and 2. Then, we investigate the adsorption kinetic and isotherm. We also studied the effect of contact time, pH, and adsorbent dose onto the adsorption capacity of MO in water.

2. Experimental Section

2.1. Materials. All the used reagents ($Zn(NO_3)_2.4H_2O$, $Al(NO_3)_3.9H_2O$, $FeCl_3$, $FeCl_2$, NaOH, HCl, aniline, ammonium persulphate) were analytical grade reagents. Methyl orange (MO) is an azo dye, with the chemical formula $C_{14}H_{15}N_3O_3S$, and molecular weight is 305.35 g/mol and is often used as an indicator. In this work, MO was used to simulate industrial wastewater in order to evaluate the adsorption capacity of Pan/MHT.

2.2. Preparation of Magnetic Hydrotalcite (MHT). MHT was preparated by coprecipitation method in the presence of Fe_3O_4 (Figure 1). An accurate amount of 0.1 g Fe_3O_4 was dispersed in distilled water (10 mL). A mixture of $Zn(NO_3)_2.4H_2O$ and $Al(NO_3)_3.9H_2O$ with Zn^{2+}/Al^{3+} molar ratio of 2.0 was dissolved in 100 mL distilled water and then coprecipitated into the Fe_3O_4 dispersion. The pH of the reaction solution was kept at around 9.5 ± 0.1. Then, the coprecipitated mixture was heated for aging at 80°C for 24 hours. The MHT was neutralized with distilled water and dried at 60°C for 6 hours obtain brown MHT powder.

2.3. Preparation of Polyaniline/MHT (Pan/MHT). Pan/MHTs were fabricated using in situ oxidative polymerization (Figure 2). An accurate amount of 0.2 g MHT was dispersed in a distilled water (40 mL) and alcohol (10 mL) mixture. 0.5 mL of Tween 80 5% was added to the mixture and then sonicated in 30 minutes to acquire a well−dispersed colloidal suspension. The desired amount of aniline dissolved in 25 mL of HCl 0.1 M. The mixture was stirred for 1 hour for complete mixing at 4°C. An accurate amount of APS ($n_{APS}/n_{aniline} = 1/5$) was dissolved in the rest of 25 mL HCl and precooled at 4°C for 15 min. APS solution was dropped into the reaction mixture and when completed, the reaction was kept at 4°C with mechanical stirring at 500 rpm. The polymerization was finished after 8 hours, then washed the suspension with a mixture of distilled water:ethanol (70 : 30) for 5 times, and dried in a vacuum dryer at 50°C for 5 hours to obtain a dark green composite Pan/MHT.

2.4. Characterization of the Composite Pan/MHT. The Fourier transform infrared (FT−IR) spectra of Pan, HT, Fe_3O_4, MHT, 0.5 Pan/MHT, 1 Pan/MHT, and 2 Pan/MHT composites were obtained using the KBr method on a Bruker Tensor 27 spectrometer, operated in 400–4000 cm^{-1} region, at 2 cm^{-1} resolution, and for 32 scans.

Figure 1: Schematic illustration of synthesis steps for MHT.

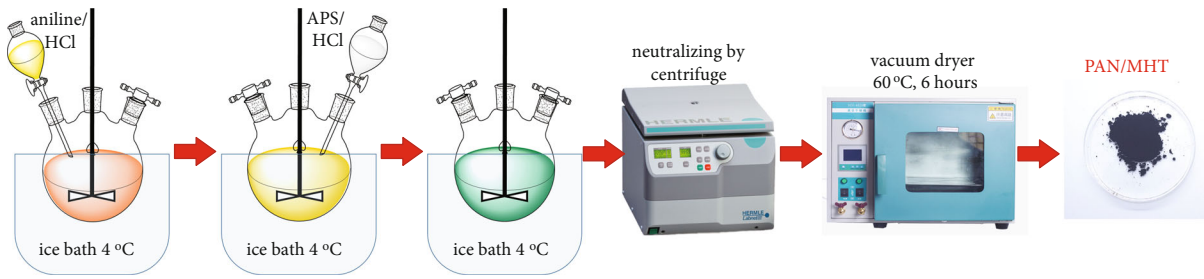

Figure 2: Schematic illustration of synthesis steps for Pan/MHT.

Powder X–ray diffraction patterns of Pan, MHT, 0.5 Pan/MHT, 1 Pan/MHT, and 2 Pan/MHT composites were obtained using a Bruker D8 Advance diffractometer with *CuKα* radiation (1,5406 Å) at room temperature in the atmospheric pressure. Data were collected in the range of 2 theta from 5 to 70° with a step of 0.02° and a scanning rate of 1°/min.

The structure and morphology of MHT, Pan, and Pan/MHT composites were observed by scanning electron microscopy (SEM). SEM observations were carried out using a Thermo Scientific E–SEM instrument.

The magnetic property of MHT and series of Pan/MHT were analyzed with a vibration sample magneparameter (VSM) method using a Lake Shore Crytotronics device.

The specific surface area and average pore size of Pan/MHT and MHT were determined by nitrogen adsorption t 76 K. The Brunauer–Emmett–Teller (BET) method was employed for the corresponding calculation.

2.5. Batch Studies. The adsorption experiments were performed using the batch equilibrium technique in aqueous solutions at room temperature. Duplicate 20 mg Pan/MHT samples were equilibrated by shaking with 25 mL of MO solution with initial concentrations (C_0) ranging between 5 mg/L and 20 mg/L and the effect of pH of MO solution ranging between 3 and 10, and the effect of the adsorbent dose was also studied. The effect of contact time was studied at 15–720 minutes, and the equilibrium was reached at 120 minutes. The MO concentration in the supernatant was measured by a UV – VIS spectrophotometer at a wavelength corresponding to the maximum absorbance for MO (460 nm) and determined using a linear regression equation obtained by plotting a calibration curve for MO over a range of concentrations. All of the adsorptions of MO in batch studies were carried out using a Jasco V630 UV – VIS spectrophotometer.

The adsorption of MO on Pan/MHT could be calculated from the difference between the initial concentration (C_0) and the equilibrium one (C_e). The adsorption was expressed in terms of adsorption percentage (%) which was calculated from the following equations:

$$\text{Adsorption\%} = \frac{C_0 - C_e}{C_0} \text{x } 100\%, \qquad C_s = \frac{C_0 - C_e}{m} \text{x V}. \tag{1}$$

where $V\,(L)$ and $m\,(g)$ represent the mass of Pan/MHTs and the volume of the suspension, respectively. Here, C_s is the capacity of MO sorption on Pan/MHT after adsorption equilibrium (mg/g).

2.6. Desorption and Reusability of Pan/MHT. For the reusability study, 0.1 g of Pan/MHT was used repeatedly for the adsorption of MO. An adsorption process was performed by adding 0.1 g Pan/MHT in 150 mL of MO at 20 mg/L and shaking for 24 hours to equilibrium adsorption. After that, the Pan/MHT was separated from the MO solution by using a magnetic bar, and the MO solution was analyzed by UV-VIS spectrophotometry to determine the MO adsorption capacity.

The desorption process was performed by dispersing Pan/MHT previously used in the adsorption process in 100 mL of HCl 1.0 M which promotes MO desorption. The desorption was performed in about 1 hour and then separating Pan/MHT by using a magnetic bar. The MO concentration in HCl was also analyzed by UV-VIS spectrophotometry. The cycles of reuse of the same Pan/MHT sample were carried out for a total of 4 cycles. The

adsorption capacity of MO and desorption MO concentration was calculated for each cycle of reuse.

3. Results and Discussion

3.1. Characterization of Composite Particles Polyaniline/Mag–HT (MHT)

3.1.1. Fourier Transform IR (FT–IR). The FT–IR characteristic of MHT as spectrum in Figure 3 shows that a strong absorption band at 1381 cm^{-1} is assigned for elongation vibration $-NO_3$ which is also present for the interlayers of MHT. The weak adsorption at about 1640 cm^{-1} is the vibration of –OH in the H_2O structure attached on the interlayer. The wide band at about 3463 cm^{-1} is characteristic for elongated vibration of –OH groups from M–OH (Al–OH, Mg–OH, and Fe–OH), lattice, and alternating layer of water: 617, 447, and 409 cm^{-1} due to elongated vibration of M–O (Al–O, Zn–O and Fe–O). Thus, Fe_3O_4 has successfully combined with HT material to fabricate MHT hybrid, and the FT–IR spectrum is consistent with that of Sulistyaningsih et al. [52].

The FT–IR infrared spectrum shown in Figure 4 clarifies the nature of the interaction between Pan and MHT in Pan/MHT materials. In the infrared (MIR) region, the peaks between 4000 and 1800 cm^{-1} are the prolonged vibration region of the O–H bonds in the hydroxyl group and N–H in the amine group. For MHT, the peak at 3447 cm^{-1} is the tensile vibration of –OH that binds the hydroxyl group surface in the structure. The adsorption peaks below 800 cm^{-1} at about 786 cm^{-1} and 618 cm^{-1} are characteristic for M–O bond (Al–O, Zn–O), and the peak at about 429 cm^{-1} is assigned for Fe–O.

Pan characterized with the strong absorptions at 3439, 2941, 1569, 1495, 1301, 1130, and 875 cm^{-1}, which was the evidence of the emeraldine form of polyaniline [53–55]. The vibration at about 3220 cm^{-1} is assigned for protonated radical cation $N-H^{+}\cdot$, and the vibration at about 3443 cm^{-1} is assigned for the N–H stretching. The characteristic band at 1515 cm^{-1} was assigned to both C=N and C–N stretching of quinoid ring structure, and the band at 1481 cm^{-1} was attributed to both C=C and C–N of benzenoid ring structure. All of these absorption peaks were characterized for the inplane bending vibration. The band at around 1301 cm^{-1} indicated the vibration of the C – N stretching of benzenoid ring, and the one at around 875 cm^{-1} was the C – H out of plane bending vibration parade-substituted benzene indicating polyaniline polymer formation. In addition, the strong band at 1130 cm^{-1} was assigned for the C – N=C group attached on the quinoid ring.

3.1.2. X-Ray Diffraction. The XRD of the MHT, Pan, 0.5 Pan/MHT, 1 Pan/MHT, and 2 Pan/MHT are measured in the range of 2θ from 5° to 70°, and the spectrums are shown in Figure 5. The XRD spectrum of MHT from Figure 3(e) has characteristic peaks of HT and some characteristic peaks of Fe_3O_4 at $2\theta = 30.1°$ and 35.5°. The characteristic peaks of MHT and HT indicate that both have layered structures with the NO_3^- anion in the interlayer. In addition, in

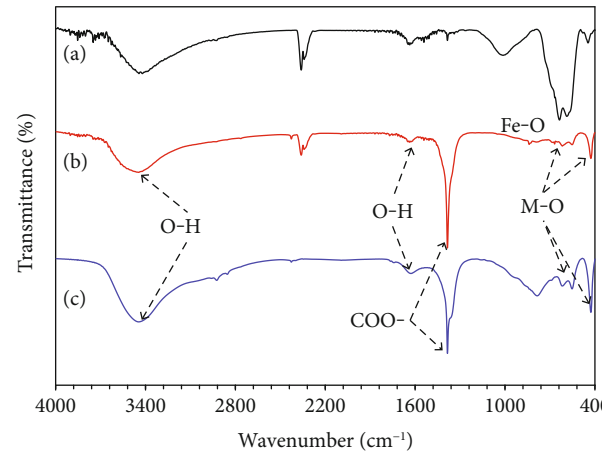

Figure 3: FT–IR spectrum of Fe_3O_4 (a), MHT (b), and HT (c).

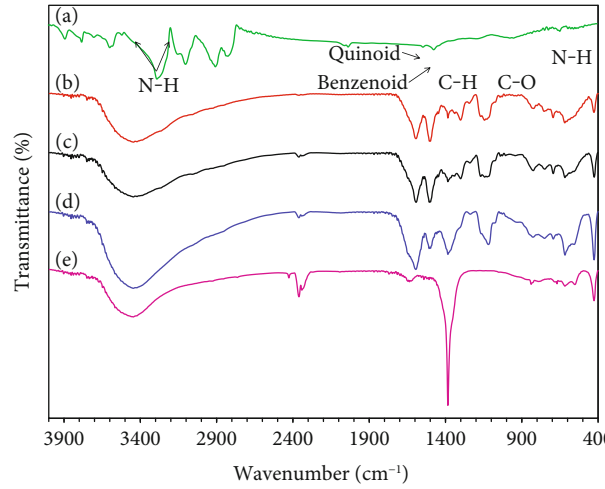

Figure 4: FT-IR spectrum of polyaniline (a), 2 Pan/MHT (b), 1 Pan/MHT (c), 0.5 Pan/MHT (d), and MHT (e).

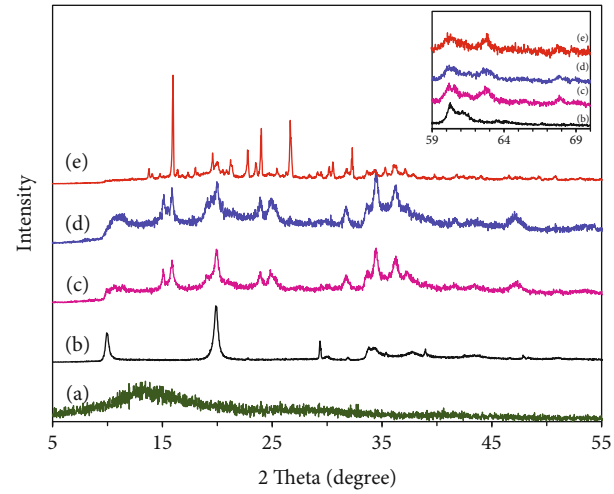

Figure 5: X-ray diffraction spectrum of polyaniline (a), 2 Pan/MHT (b), 1 Pan/MHT (c), 0.5 Pan/MHT (d), and MHT (e).

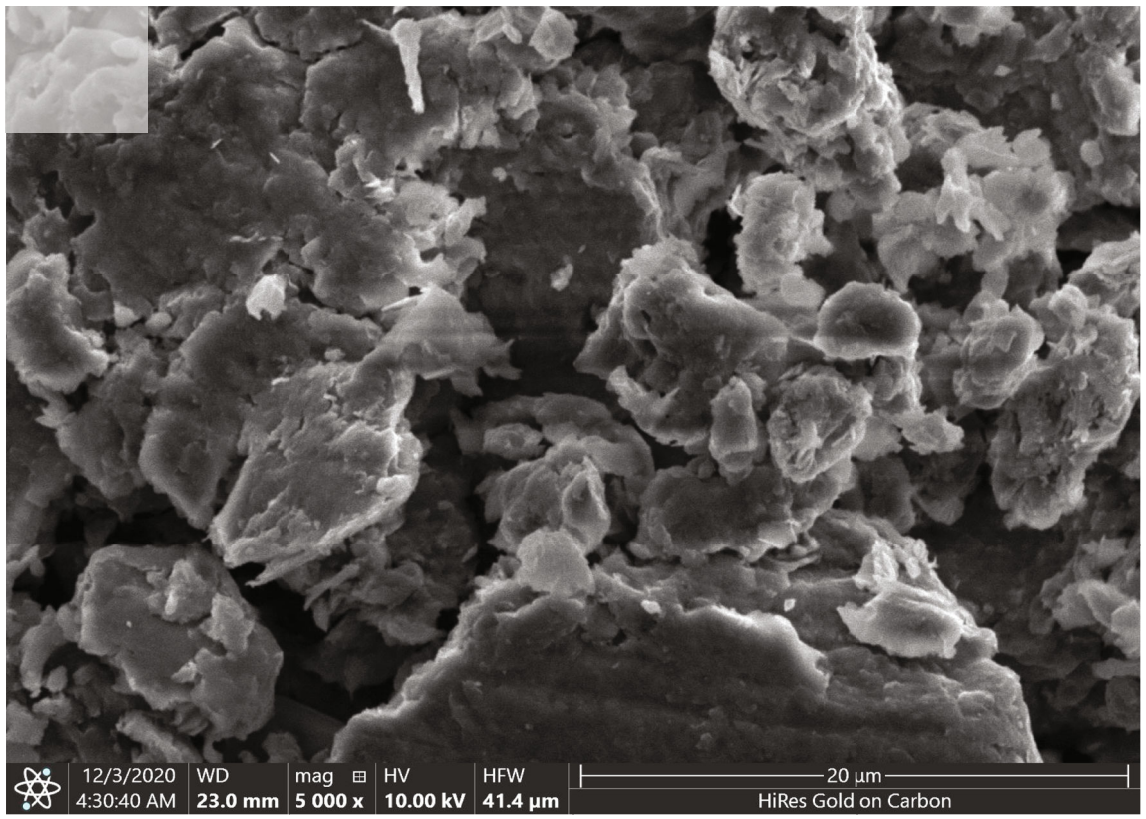

(a)

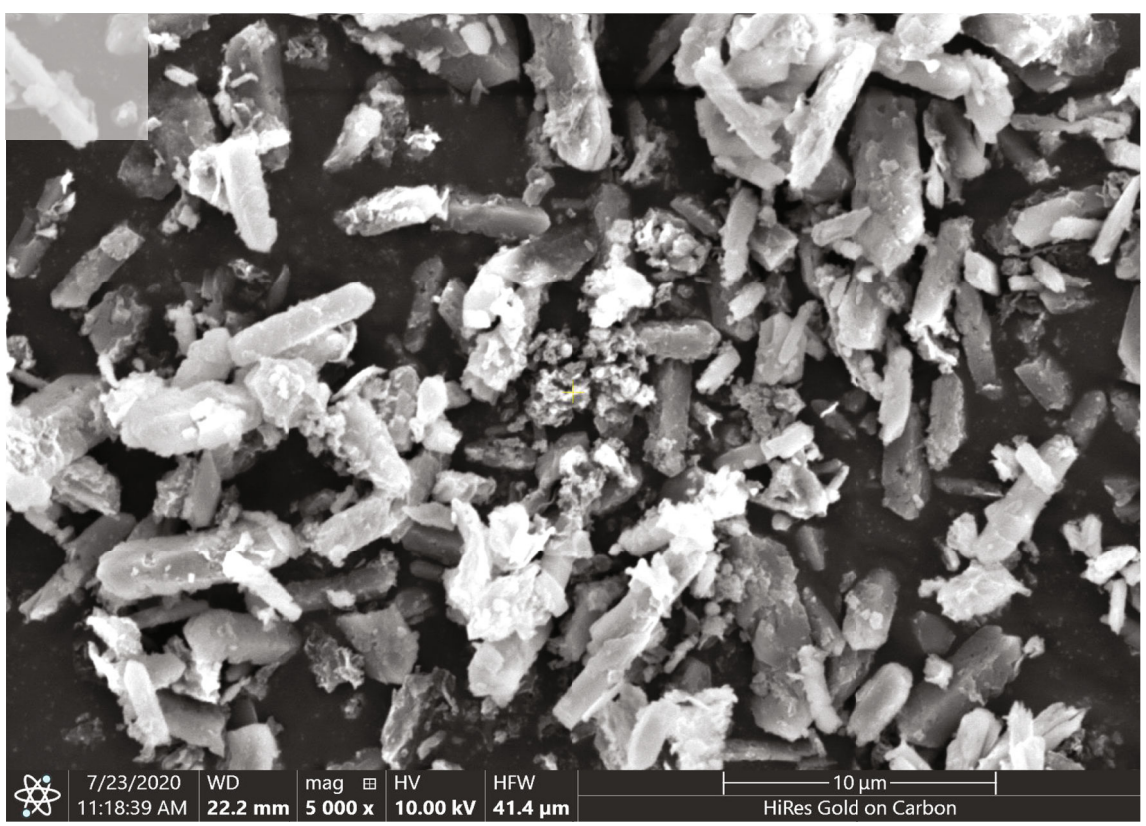

(b)

Figure 6: Continued.

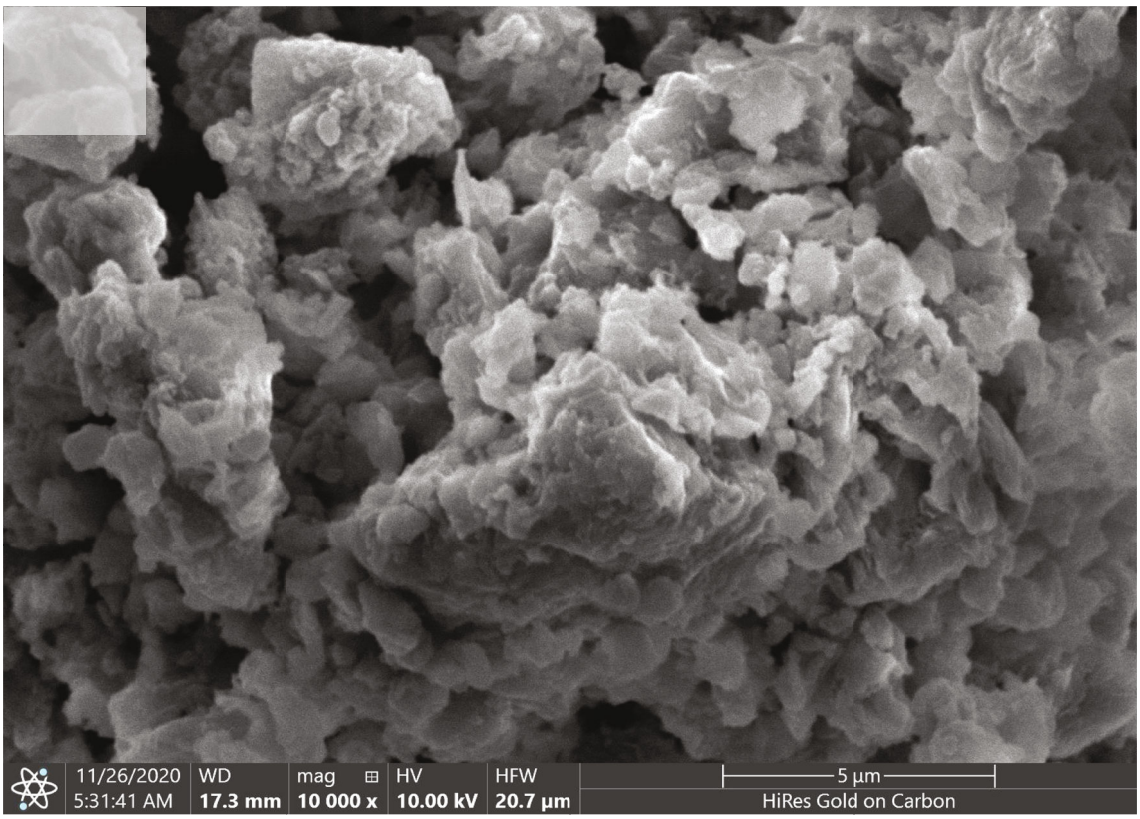

(c)

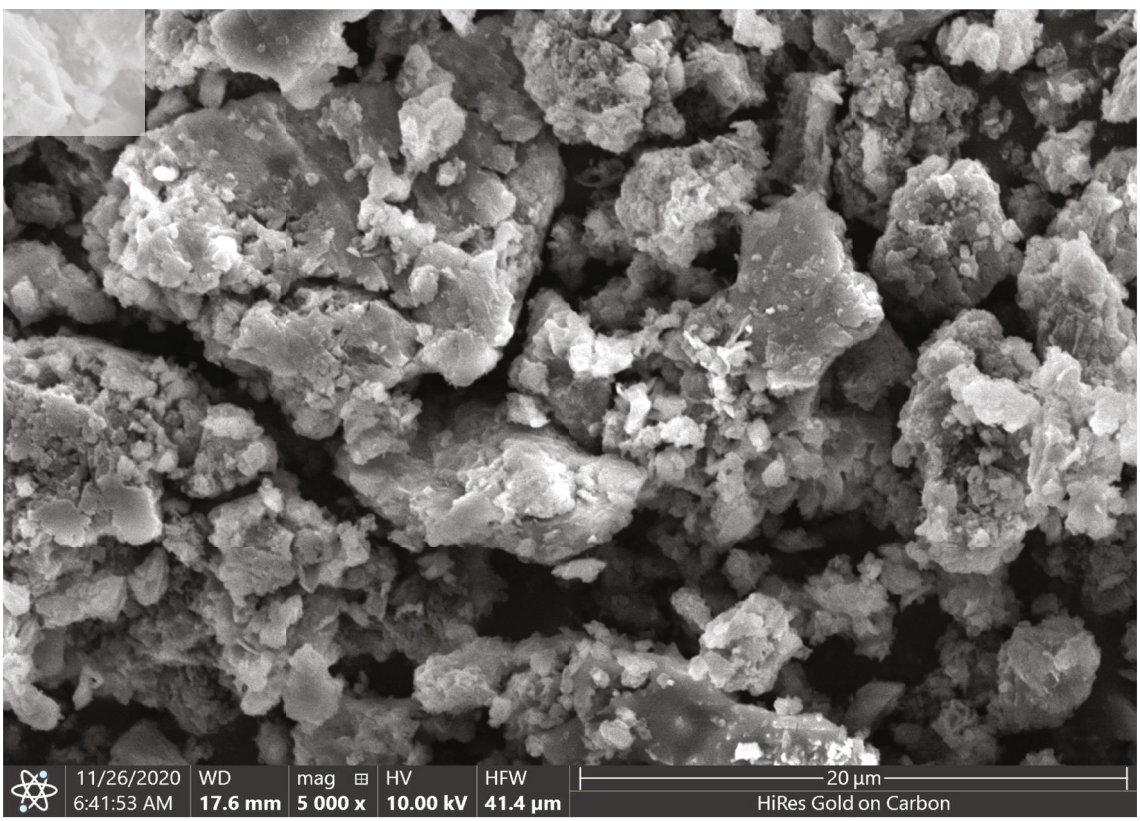

(d)

Figure 6: Continued.

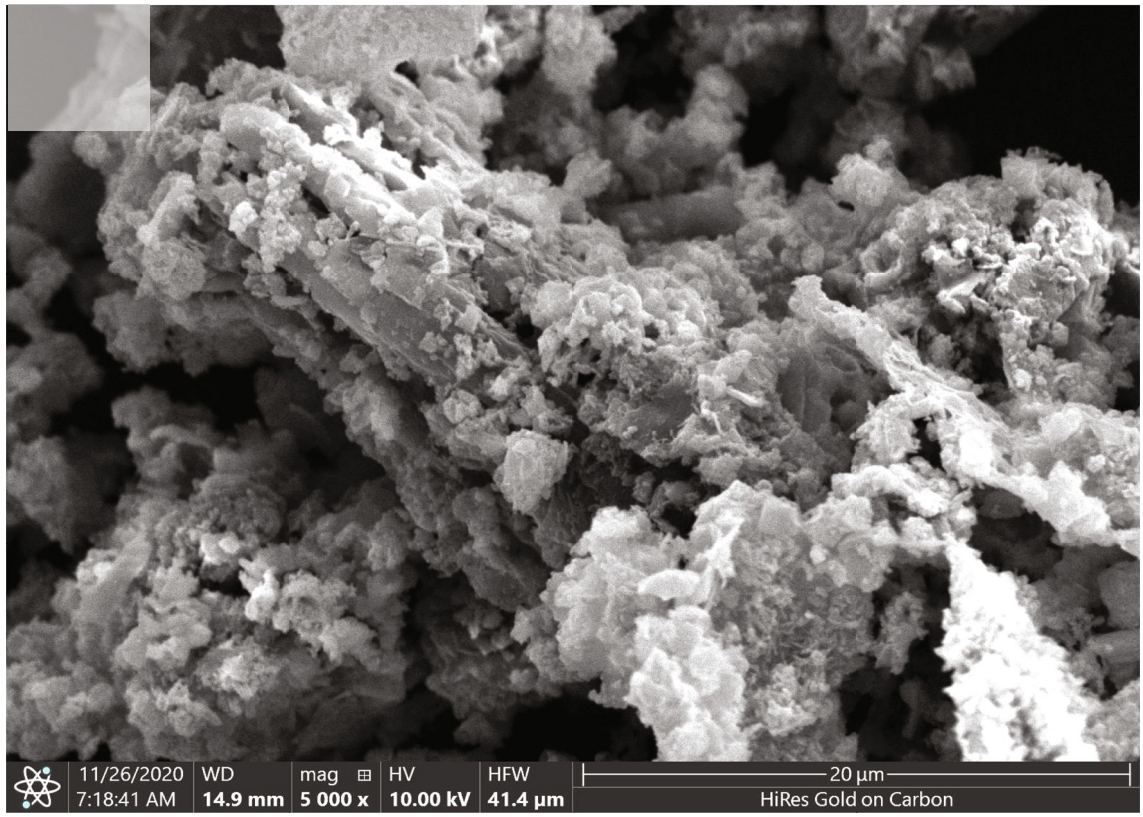

(e)

Figure 6: SEM images of MHT (a), polyaniline (b), 0.5 Pan/MHT (c), 1 Pan/MHT (d), and 2 Pan/MHT (e).

MHT material, the 34.6° peak that appeared in HT is divided into two subpeaks. The first peak at a smaller diffraction angle shows the peak of the hydrotalcite, and the second one at a slightly larger diffraction angle shows the magnetite core deposited on the surface of the hydrotalcite corresponding to the magnetite particle combined on the surface of HT. XRD diffraction spectra of MHT material are consistent with that of Sulistyaningsih et al. [52].

The results from the figure show the characteristic diffraction peak of Pan at $2\theta = 13°$, $2\theta = 21°$, and $2\theta = 25°$. Typical diffraction peaks of MHT at $2\theta = 11.7°$, $2\theta = 11.8°$, and $2\theta = 11.6°$. With different from ratios of $m_{\text{Pan}}/m_{\text{MHT}}$, there is also different typical diffraction peak of MHT at $2\theta = 11.6°$ and $2\theta = 12°$. It is because of the bond between Pan and MHT in the material, and the interaction between Pan and MHT can be influenced by hydroxides groups on the MHT surface, affecting the structure and material properties.

3.1.3. SEM Images. The morphology of the material was observed by SEM images in Figure 6. Pan/MHT morphology was observed, in which the distribution of Pan and MHT differed markedly in the proportions. The structural morphology of MHT is a porous material consisting of multilayers, and Pan has the structure of a long carbon chain. The distribution of MHT for Pan is different when changing the mass ratio of Pan. This result is completely consistent with the results of structural analysis by significantly reduced X−ray diffraction.

3.1.4. Vibrating Sample Magnetometer (VSM) Analysis. The magnetic properties of MHT and series of Pan/MHT were investigated using a vibrating sample magnetometer at room temperature, and the magnetization curves of MHT and series of Pan/MHT were shown in Figure 7. The roughly coincident hysteresis curves show that the grain size of the MHT metal phase is very small, nanometers in size and is a superparamagnetic material. Because MHT is the hybrid material from HT with only 1 wt% Fe_3O_4 particle, the superparamagnetic characteristic of MHT is the low value of Ms and Mr that are 2.73×10^{-3} emu/g and 0.10×10^{-3} emu/g, and H_c is 20.06 Oe. Pan is a conductive polymer, and it tends to help increasing the ferromagnetic behavior for MHT. However, Pan is diamagnetic, so that when the mass ratio of $m_{\text{Pan}}/m_{\text{MHT}}$ increased, the values of M_s and M_r decreased as the results in Table 1. And this result is consistent with the announcement of Umare et al. and Jokar et al. [56, 57]. These magnetic properties are high enough that Pan/MHT materials can be separated from the solution by an external magnet.

The low M_r value indicates that the Pan/MHT can be easily separated from the solution by an external magnetic field and redistributed into the solution after the magnetic field is disconnected. This will be an advantage for the separation, recovery, and reuse of the adsorbent as well as the

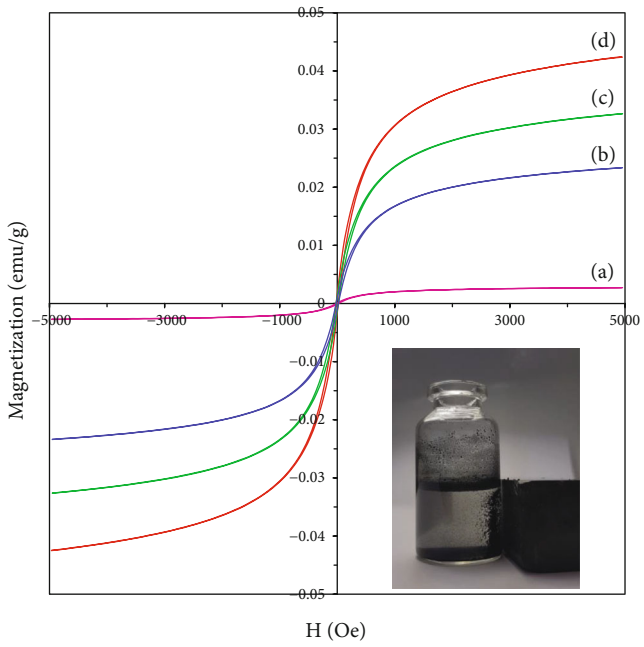

Figure 7: Magnetization vs. applied magnetic field for MHT (a), 2 Pan/MHT (b), 1 Pan/MHT (c), and 0.5 Pan/MHT (d).

Table 1: Magnetic parameters of MHT and Pan/MHT composites.

Sample	H_c (Oe)	M_s (emu/g)	M_r (emu/g)
MHT	20.06	2.73×10^{-3}	0.10×10^{-3}
0.5 Pan/MHT	17.19	42.46×10^{-3}	1.59×10^{-3}
1 Pan/MHT	18.09	32.64×10^{-3}	1.29×10^{-3}
2 Pan/MHT	18.56	23.38×10^{-3}	0.91×10^{-3}

catalyst. MHT has the lowest M_s and M_r which are 2.73×10^{-3} emu/g and 0.10×10^{-3} emu/g. When combined with Pan, the M_r value of composites was decreased, but increasing the mass ratio of $m_{\text{Pan}}/m_{\text{MHT}}$ helped to decrease the M_s and M_r values. In particularly, the M_r values of 0.5 Pan/MHT, 1 Pan/MHT, and 2 Pan/MHT are 1.59×10^{-3}, 1.29×10^{-3}, and 0.91×10^{-3} emu/g, respectively. Then, the M_s values of 0.5 Pan/MHT, 1 Pan/MHT, and 2 Pan/MHT are 42.46×10^{-3}, 32.64×10^{-3}, and 23.38×10^{-3} emu/g, respectively.

3.1.5. Bruanauer–Emmett–Teller (BET). The surface area is well known to be important for adsorption performance. While the pore size of MHT and 2 Pan/MHT is the same which are 26.2 Å and 24.6 Å, the BET surface areas of MHT and 2 Pan/MHT were calculated to be 2.796 m^2/g and 15.460 m^2/g. The higher surface of 2 Pan/MHT provides more active sites for MO adsorption. This result is consistent with the morphology of MHT and Pan/MHT from the SEM images in Figure 8.

3.2. Effect of Contact Time and Kinetic Adsorption

3.2.1. Effect of Contact Time. Figure 9 shows the effect of contact time of 0.5 Pan/MHT, 1 Pan/MHT, and 2 Pan/MHT with 100 mL of 20 mg/L MO solution. The adsorption amounts of MO increased rapidly in the initial 30 minutes for all samples. Then, the adsorption amounts increased slighter in the next 30 minutes. It becomes slow to attained equilibrium time which is 120 minutes for 0.5 Pan/MHT, 1 Pan/MHT, and 240 minutes for 2 Pan/MHT in the same conditions. The difference of equilibrium time for MO adsorption obtained by various adsorbents can be explained by the MO anion adsorption on the adsorbents by surface and anion exchange mechanism. The adsorbent with the higher mass ratio of Pan/MHT, the more MO can be adsorbed. This result is due to the complex adsorption mechanism of Pan such as surface adsorption, anion −exchange, …, which is consistent with the research of Monika et al. and Wang et al. [58, 59].

Kinetic modeling of the adsorption process provides a prediction of adsorption rates and allows the determination of suitable rate expressions characteristic of the possible reaction mechanisms. In this study, the most frequently used models, the pseudofirst−order, the pseudosecond−order, and the intraparticle diffusion model were tested.

Pseudofirst−order kinetics: the linearized from of the pseudofirst−order linearized equation is given as

$$\log (Q_e - Q_t) = \log\ Q_e - \frac{k_1}{2.303} t, \tag{2}$$

where t and Q_e (mg/g) are the MO removal at time t and at equilibrium. k_1 (min^{-1}) is the equilibrium rate constant of the pseudofirst-order equation. The plots of $\log (Q_e - Q_t)$ vs. t are shown in Figure 10(a), and k_1 is predicted Q_e can be determined from the slope and intercept of the plot, respectively.

Pseudo−secondorder kinetics: the linearized form of the pseudosecond-order equation is given as

$$\frac{t}{Q_t} = \frac{t}{Q_e} + \frac{1}{k_2 Q_e^2}, \tag{3}$$

where k_2 [g/(mg min)] is the equilibrium rate constant of the pseudosecond−order equation. The plot of t/Q_t vs. t is shown in Figure 10(b), and k_2 and Q_e can be determined from the slope and intercept of the plot, respectively.

Intraparticle diffusion model: the intraparticle diffusion model assumes that film diffusion is negligible, and the only rate-controlling step is intraparticle diffusion in the adsorption process [60]. Hence, the adsorbed amount at time t should be directly proportional to $t^{0.5}$ rather than t. The model is given as

$$Q_t = k_{\text{id}} t^{0.5} + C, \tag{4}$$

where k_{id} is the intraparticle diffusion rate constant (mg/g $\text{min}^{0.5}$), which can be calculated from the slope of the linear plot of Q_t vs. $t^{0.5}$ and can be determined from the slope of the plot shown in Figure 10(c).

The kinetic parameters obtained from the application of different models are shown in Table 2. The pseudosecond

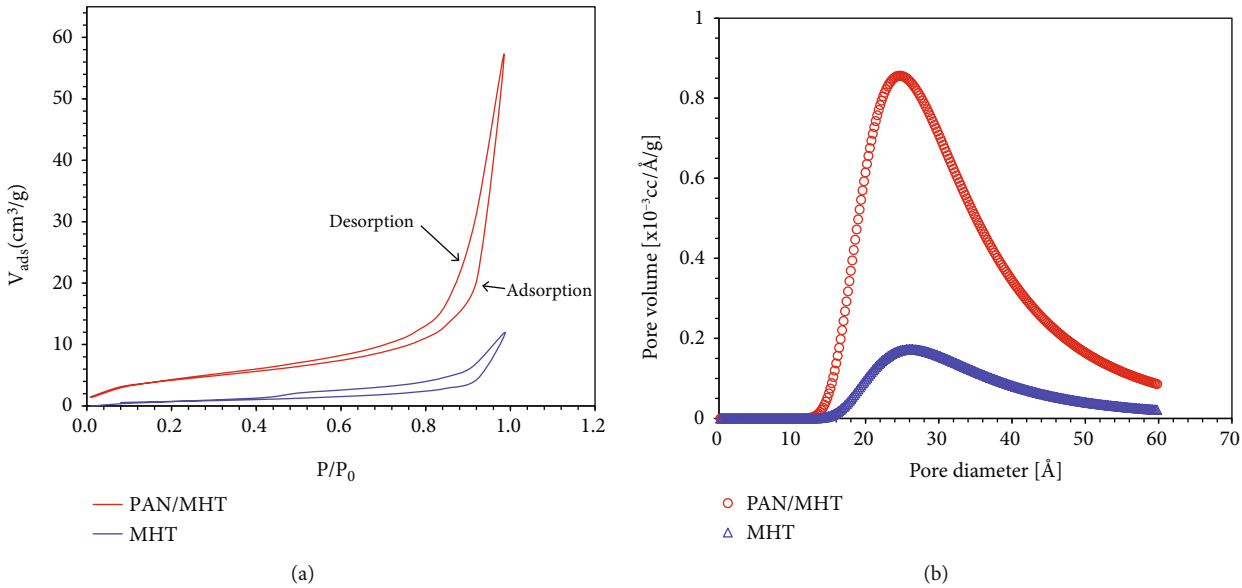

Figure 8: Nitrogen adsorption–desorption isotherms (a) and pore disstribution (b) of MHT and 2 Pan/MHT.

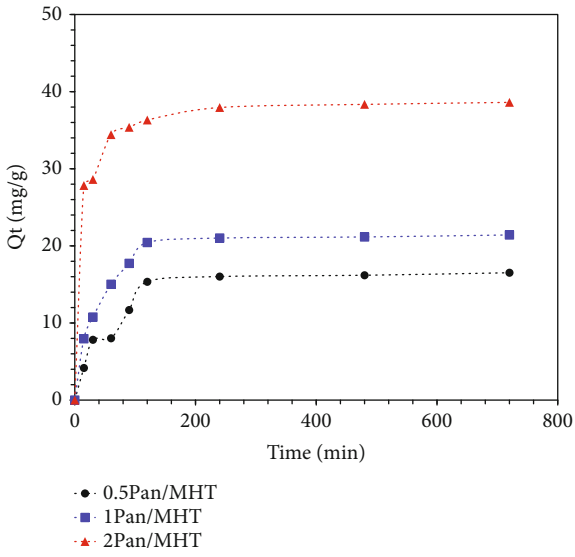

Figure 9: Effect of contact time on MO adsorption onto 0.5 Pan/MHT, 1 Pan/MHT, and 2 Pan/MHT.

–order model is the most suitable in describing the adsorption kinetics of MO in all three Pan/MHT composites, based on the correlation coefficient ($R^2 = 0.994$, 0.998, and 0.999 corresponding to 0.5 Pan/MHT, 1 Pan/MHT, and 2 Pan/MHT), and the experimental and calculated values of Q_e are not much different.

3.2.2. Effect of pH on the MO Adsorption. The result from Figure 11 shows that the adsorption efficiency of all three materials decreases gradually according to the pH value of the solution, the efficiency reaches the highest and most stable value at pH from 3 – 4, to pH 5, and the efficiency productivity started to decrease gradually. This is related to the surface area of the material, the presence of hydroxyl groups (OH–) on the surface of the material, and the exchange of protons (H+). This group is both capable of giving and receiving protons according to the pH of the solution when in solid–phase contact. The process of receiving protons on the surface takes place in an acid environment, while proton transfer occurs in an alkaline environment.

3.3. Adsorption Isotherms

3.3.1. Effect of Initial Concentration of MO on Sorption of MO. The effect of initial concentration on MO adsorption onto 0.5 Pan/MHT, 1 Pan/MHT, and 2 Pan/MHT is shown in Figure 12. The experiment was performed with a constant adsorbent dose of 20 mg/25 mL MO. The adsorption capacity of MO increased when increasing the initial MO concentration. The Q_e values of 2 Pan/MHT are always higher than ones of 0.5 Pan/MHT and 1 Pan/MHT. This can be due to the structure of 2 Pan/MHT with high surface area as the result analyzed from BET and SEM methods above. For a solid-liquid system, the equilibrium of adsorption is one of the important physic-chemical aspects in the description of adsorption behavior. In this work, the models of Langmuir [61] and Freundlich [62] isotherm are evaluated. The results obtained from the different models provide the behavior of the adsorption mechanisms and the surface properties and affinities of the adsorbent.

The Langmuir isotherm is used to describe the equilibrium between the surface of the solid and the solution and is valid for monolayer adsorption onto a surface with a finite number of identical sites. The Langmuir model equation is given as

$$\frac{C_e}{Q_e} = \frac{1}{Q_m b} + \frac{C_e}{Q_m}, \quad (5)$$

where Q_m (mg/g) is the maximum monolayer adsorption

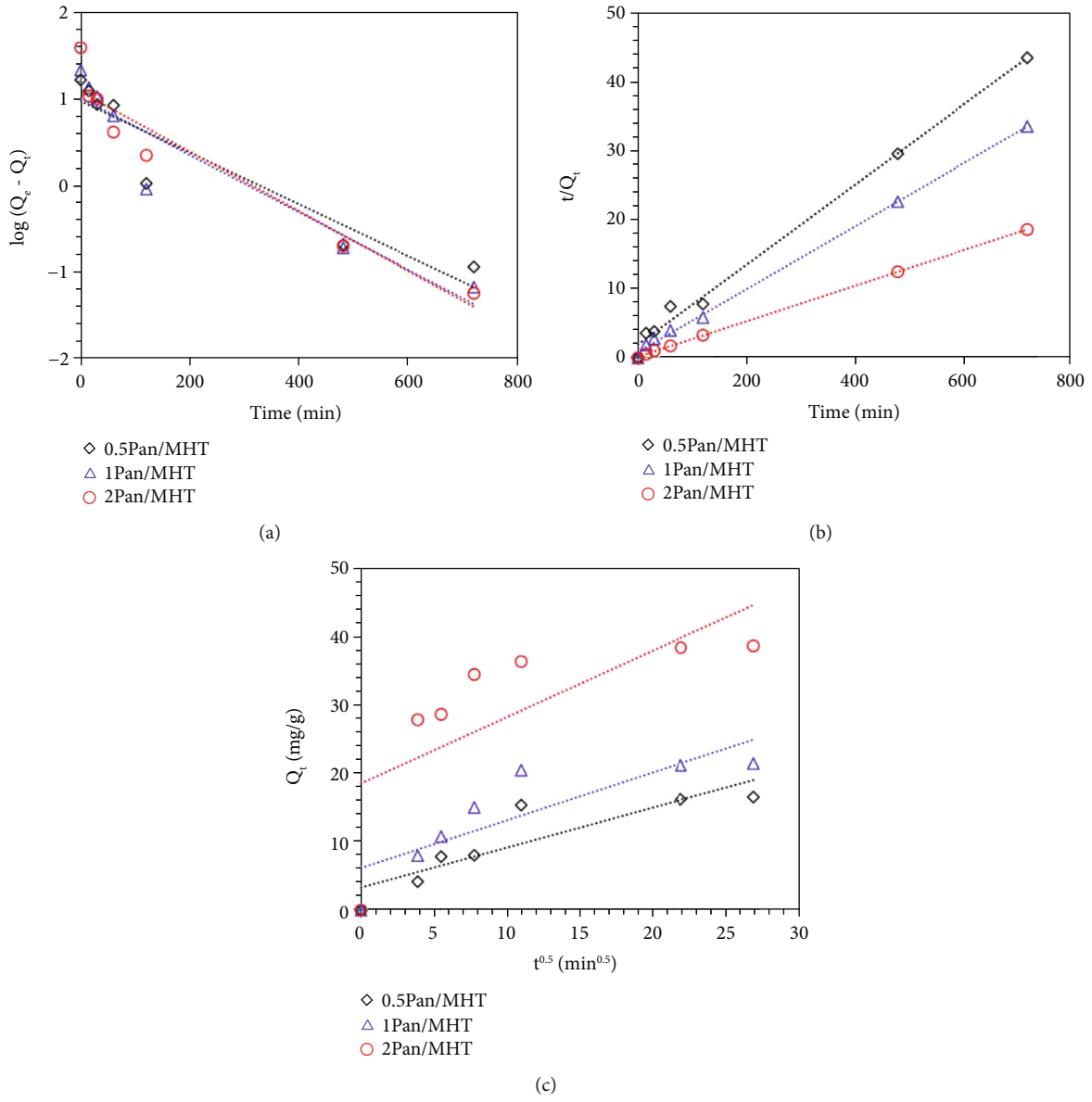

FIGURE 10: MO adsorption kinetics by 0.5 Pan/MHT, 1 Pan/MHT, and 2 Pan/MHT adsorbents. Pseudofirst−order model (a), pseudosecond −order model (b), and intraparticle diffusion model (c).

TABLE 2: Kinetic parameters of MO adsorption on Pan/MHT composite.

Adsorbents	$Q_{e,exp}$ (mg/g)	Pseudofirst−order			Pseudosecond−order			Intraparticle diffusion		
		$Q_{e,cal}$ (mg/g)	k_1 (min^{-1})	R^2	$Q_{e,cal}$ (mg/g)	k_2 g/(mg min)	R^2	k_{id} Mg/g $min^{0.5}$	C	R^2
0.5 Pan/MHT	16.52	10.63	0.008	0.837	19,92	0.004	0.994	0.195	2.036	0.748
1 Pan/MHT	21.42	11.32	0.009	0.821	25,77	0.002	0.998	0.208	3.787	0.709
2 Pan/MHT	38.61	12.91	0.009	0.855	34,72	0.009	0.999	0.174	11.38	0.742

capacity, and b (L/mg) is the Langmuir constant related to the binding energy. The plots of C_e vs. C_e/Q_e are shown in Figure 13(a), and the values of Q_m and b are calculated from the slope and intercept of the plots, respectively.

The Freundlich isotherm is an empirical equation that assumes that the adsorprion face becomes heterogeneous during the course of the adsorption process. The linearized form of the Freundlich model is given as

$$\log Q_e = \log k_f + \frac{1}{n} \log C_e, \tag{6}$$

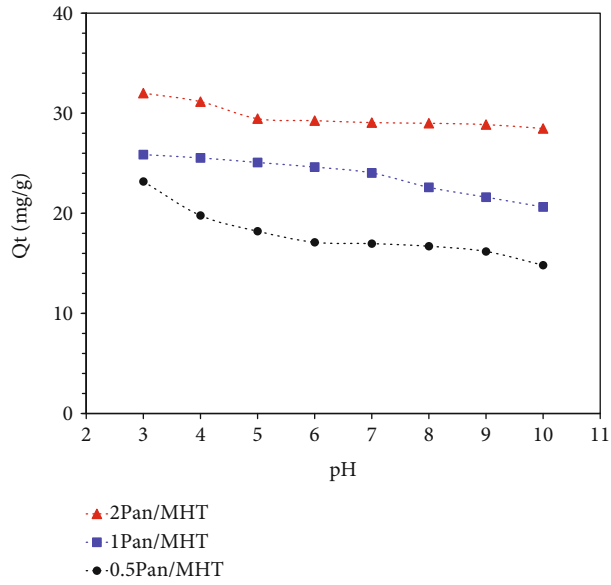

Figure 11: Effect of pH on MO adsorption onto 0.5 Pan/MHT, 1 Pan/MHT, and 2 Pan/MHT.

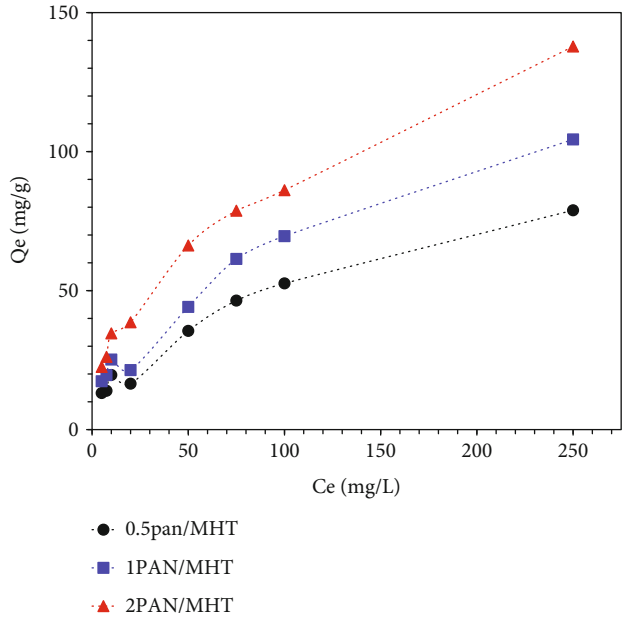

Figure 12: Effect of initial MO concentration on MO adsorption onto 0.5 Pan/MHT, 1 Pan/MHT, and 2 Pan/MHT.

where k_f (mg/g) and n are the Freundlich constants related to adsorption capacity and adsorption intensity, respectively. The plots of log C_e vs. log Q_e were shown on Figure 13(b), and the values of $1/n$ and k_f are calculated from the slope and intercept of the plots, respectively.

All the correlation coefficients, R^2 values, and the constants calculated from Langmuir and Freundlich models are listed in Table 3. The R^2 of both Langmuir and Freundlich models of all three adsorbents is higher than 0.91; so, the adsorption of MO onto Pan/MHT composite appropriate with either monolayer of dyeing molecules covers the Pan/MHT surface or interaction between adsorbents and MO molecules. All three R^2 values of the Freundlich model of Pan/MHT composites are higher than R^2 of the Langmuir model. In particularly, $R^2 = 0.9506, 0.9472$, and 0.9912 corresponding to 0.5 Pan/MHT, 1 Pan/MHT, and 2 Pan/MHT. In addition, the n values of three composites are higher than 2 ($n = 2.0973, 2.119$, and 2.1872 for 0.5 Pan/MHT, 1 Pan/MHT, and 2 Pan/MHT, respectively) which indicates that the MO adsorption on Pan/MHT composite is not only monolayer surface adsorption. The mechanism of MO adsorption onto Pan/MHT composite is either of the surface adsorption or other types of interactions, such as electrostatic interaction, ion exchange, hydrogen bonding, and van der Waals forces. In all three composites, 2 Pan/MHT is the most suitable for the Freundlich model and the Langmuir model too. The MO adsorption capacity of 2 Pan/MHT is also the highest with $Q_e = 156.25$ mg/g.

Dubinin-Radushkevich (D-R) isotherm is generally used to describe the sorption isotherms of a single solute system (Figure 13(c)). The D-R isotherm can also help to confirm that the adsorption process was chemisorption or physical adsorption [63]. D-R equation is represented as follows:

$$\ln Q_e = \ln Q_m - \beta\varepsilon^2 \tag{7}$$

where Q_e is equilibrium adsorbent-phase concentration of adsorbate (mg/g), and Q_m is theoretical saturation capacity (mg/g). The plots of ε^2 vs. ln Q_e were shown in Figure 10(c), and the values of β and ln Q_m are calculated from the slope and intercept of the plots, respectively. β is the activity coefficient related to the mean free energy of adsorption (mol^2/kJ^2), and ε is the polanyipotential (kJ/mol).

$$\varepsilon = \mathrm{RTln}(1 + 1/\mathrm{C_e}), \tag{8}$$

where R is the universal gas constant (8.314 J/mol.K), T is the Kelvin temperature (K), and C_e is the equilibrium aqueous phase concentration of adsorbate (mg/L).

The D-R model is mainly used to estimate the average free energy of adsorption (kJ/mol)

$$\mathrm{E} = \frac{1}{\sqrt{2\beta}}, \tag{9}$$

when $E < 8$ kJ/mol, the adsorption is physical adsorption and when $E > 8$ kJ/mol, the adsorption is chemisorption [64]. The adsorption energy values (E) of 0.5 Pan/MHT, 1 Pan/MHT, and 2 Pan/MHT are under 8 kJ/mol. In particularly, $E = 0.273, 0.277$, and 0.269 kJ/mol corresponding to 0.5 Pan/MHT, 1 Pan/MHT, and 2 Pan/MHT. This result indicates that the adsorption process of MO on three kinds of Pan/MHT composites is physical adsorption.

3.3.2. Effect of 2 Pan/MHT Dosage on the Sorption of MO. The result from Figure 14 shows the adsorption efficiency (H %) when using a different dose of 2 Pan/MHT (0.01, 0.02, and 0.03 g) and shows the adsorption efficiency increases when increasing 2 Pan/MHT dose.

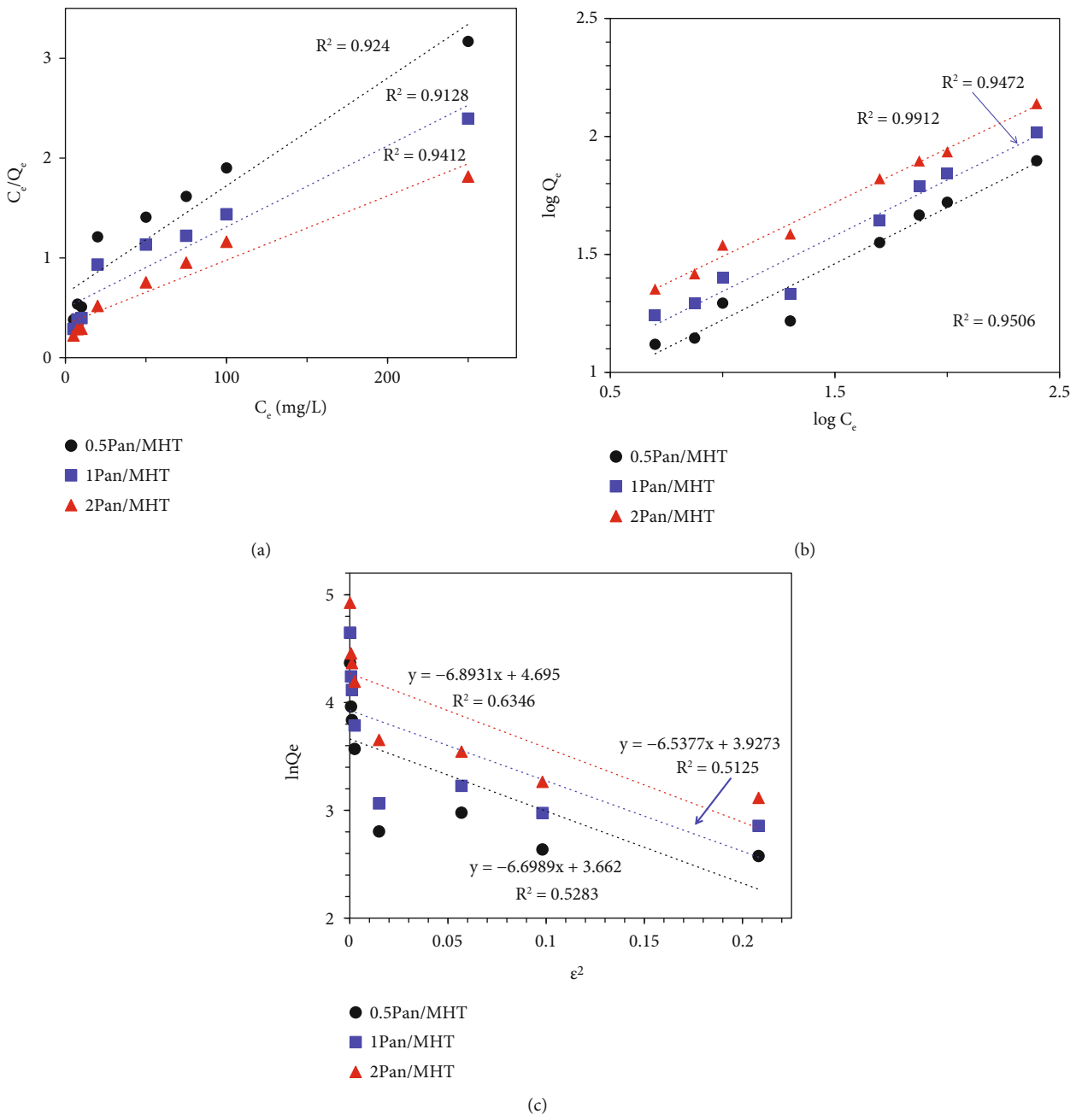

Figure 13: Adsorption isotherms of MO on Pan/MHT composites with Langmuir isotherm model (a), Freundlich isotherm model (b), and Dubinin-Radushkevich isotherm model (c).

Table 3: Fitting parameters of adsorption isotherms for MO on Pan/MHT composites.

Adsorbents	Langmuir isotherm			Freundlich isotherm			Dubinin-Radushkevich			
	Q_m (mg/g)	b (L/mg)	R^2	n	k_f (mg/g)	R^2	Q_m (mg/g)	β (mol^2/kJ^2)	R^2	E (kJ/Mol)
0.5Pan/MHT	92.59	0.017	0.924	2.097	5.562	0.951	38.93	6.699	0.528	0.273
1 Pan/MHT	123.5	0.016	0.913	2.119	7.437	0.947	50.77	6.538	0.513	0.277
2 Pan/MHT	156.3	0.019	0.941	2.187	10.81	0.991	71.49	6.893	0.635	0.269

For all 3 doses of 2 Pan/MHT, MO was immediately adsorbed on 2 Pan/MHT and after 30 minutes, the adsorption efficiency obtained 55.39%, 63.88%, and 65.97% according to use of 0.01, 0.02, and 0.03 g of 2 Pan/MHT, respectively. Then, the adsorption efficiency increase slightly and reached to equilibrium after 240 minutes with the

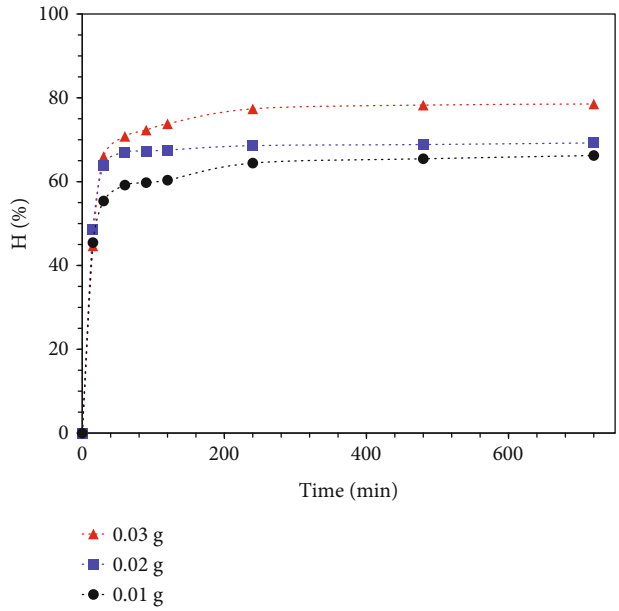

Figure 14: Effect of adsorbent dose in MO adsorption onto 2Pan/MHT composite.

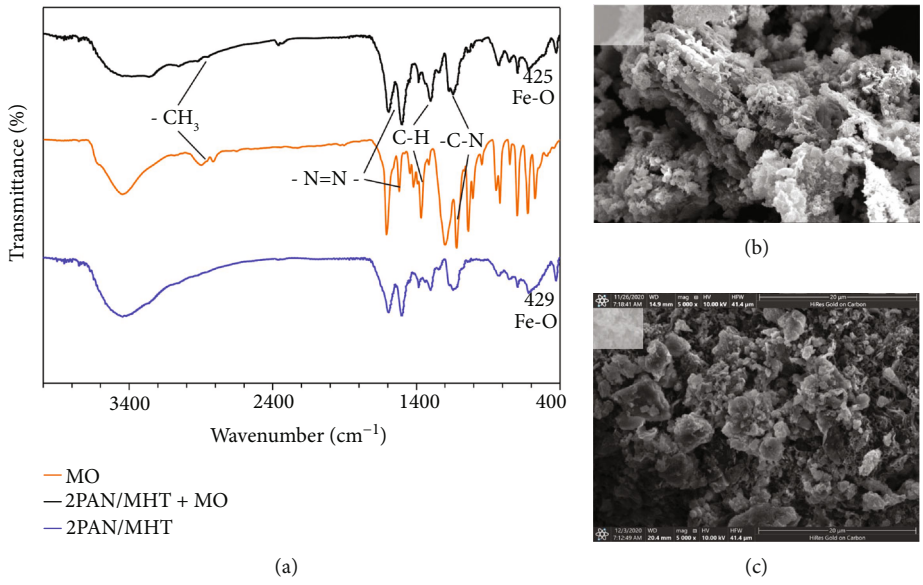

Figure 15: FT-IR spectra of MO (red line), 2 Pan/MHT (blue line), and 2 Pan/MHT after adsorption of MO (—) (a), SEM images of 2 Pan/MHT (b), and 2 Pan/MHT after adsorption of MO (c).

adsorption efficiency obtained 64.43%, 68.59%, and 77.37% according to the use of 0.01, 0.02, and 0.03 g of 2 Pan/MHT, respectively. This result is expected because the increase of adsorbent dose leads to a greater surface area.

The FT–IR spectra of MO, 2 Pan/MHT, and 2 Pan/MHT after adsorption of MO are shown in Figure 15(a). MO is characterized by the peak at 2896 cm^{-1} for asymmetric CH_3 stretching vibration; the peaks at 1520 cm^{-1} and 1421 cm^{-1} are assigned for C=C–H in plane CH bend; peak at 817 cm^{-1} is characteristic of the benzene ring. The peak at 1608.32 cm^{-1} is assigned for –N=N–, and the peaks at 1201 cm^{-1} and 1121 cm^{-1} are assigned for –C–N. The peaks at 697 cm^{-1}, 623 cm^{-1}, and 574 cm^{-1} are assigned for the stretching vibration -C-S-, and the peak at 1367 cm^{-1} is assigned for the stretching vibration S=O. These characteristics also exist on Pan/MHT materials after adsorption, demonstrating the presence of MO dye on the material, and this result is consistent with the announcement of Harikumar et al. [65].

SEM images of 2 Pan/MHT and 2 Pan/MHT after adsorption of MO (Figures 15(b) and 15(c)) clearly show the material surface before and after MO adsorption. The surface and pores of 2 Pan/MHT after adsorption of MO are covered with the MO (adsorbed components), and the

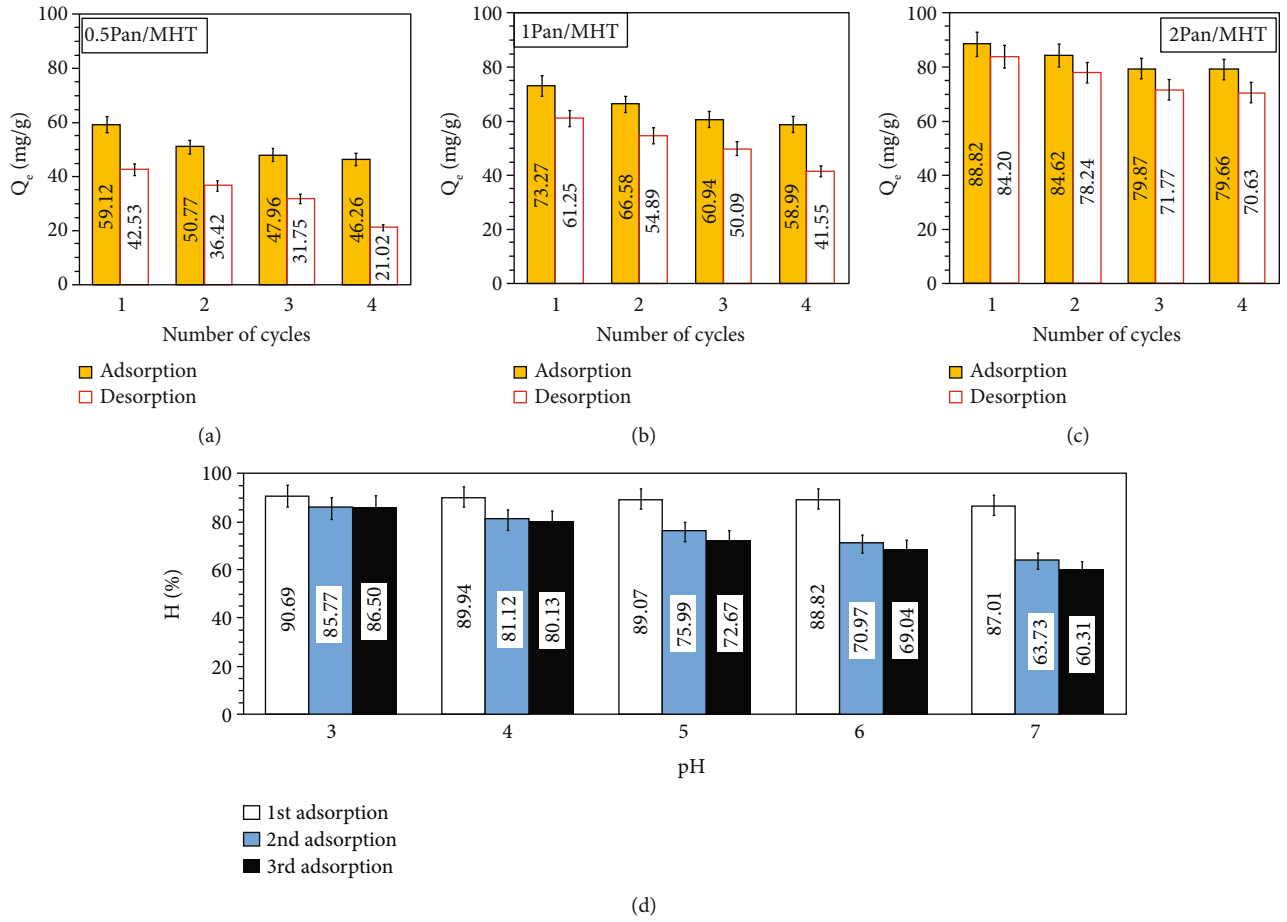

Figure 16: MO adsorption and desorption cycles with 0.5 Pan/MHT (a), 1 Pan/MHT (b), 2 Pan/MHT (c), and the effect of solution pH on the reusability of 2 Pan/MHT for MO adsorption (d).

result is the surface of the material more homogeneous than the original. It is mean that the material samples after adsorption have almost filled gaps.

3.4. Desorption of MO and Reusability of Pan/MHT. Another parameter that defines the functionality of adsorbent material is its capacity to be regenerated and reused in several adsorption and desorption cycles. For this reason, MO adsorption and desorption experiments were performed with Pan/MHT by using a 0.1 M HCl solution as an eluent. This eluent was chosen because in acid conditions, Pan is in emeraldine salt and is doped with H+ ions, and MO is in its cationic form [66, 67]. Therefore, due to electrostatic repulsions, the MO molecules would be desorbed from the composite structure.

Figure 16 shows the adsorption and desorption efficiency of MO after 4 cycles. The result show that the MO adsorption decreases to 12.86%, 14.28%, and 9.16% according to using 0.5 Pan/MHT, 1 Pan/MHT, and 2 Pan/MHT. The MO desorption from 0.5 Pan/MHT, 1 Pan/MHT, and 2 Pan/MHT also decreases to 21.51%, 19.7%, and 13.57%, respectively. This can be due to the increase of Pan in a composite structure, which enhances both adsorption and desorption of MO on the adsorbent. Thus, Pan/MHT surface can be regenerated without a problem. Although MO is completely desorbed, the adsorption percentage decreases, and this behavior is because of the loss of Pan due to stirring and material management. Therefore, this material can be reused in multiple cycles if it wants to be coupled to a recirculation system.

The results show that at a low pH 3 – 4, the MO adsorption capacity (H %) obtained over 80% after 3 cycles of reuse. When the solution pH > 5 – 7, the MO adsorption decreased and obtained 60– 73% efficiency of MO removal after 3 cycles of reuse. This shows that the MO adsorption and desorption are suitable for performance in acidic environments at pH 3 – 4.

3.5. Mechanism of Adsorption. With all the results above, the process of adsorption, recovery, and desorption of MO on Pan/MHT was described as Figure 17(a). The adsorption and desorption mechanism of MO on Pan/MHT are the combination of chemisorption and physical adsorption, which can be illustrated in Figures 17(b)–17(d) and explained as below:

(i) In solution, MO molecule is dissociated into M-SO_3^- with M is an organic part of dyeing molecule. Pan is

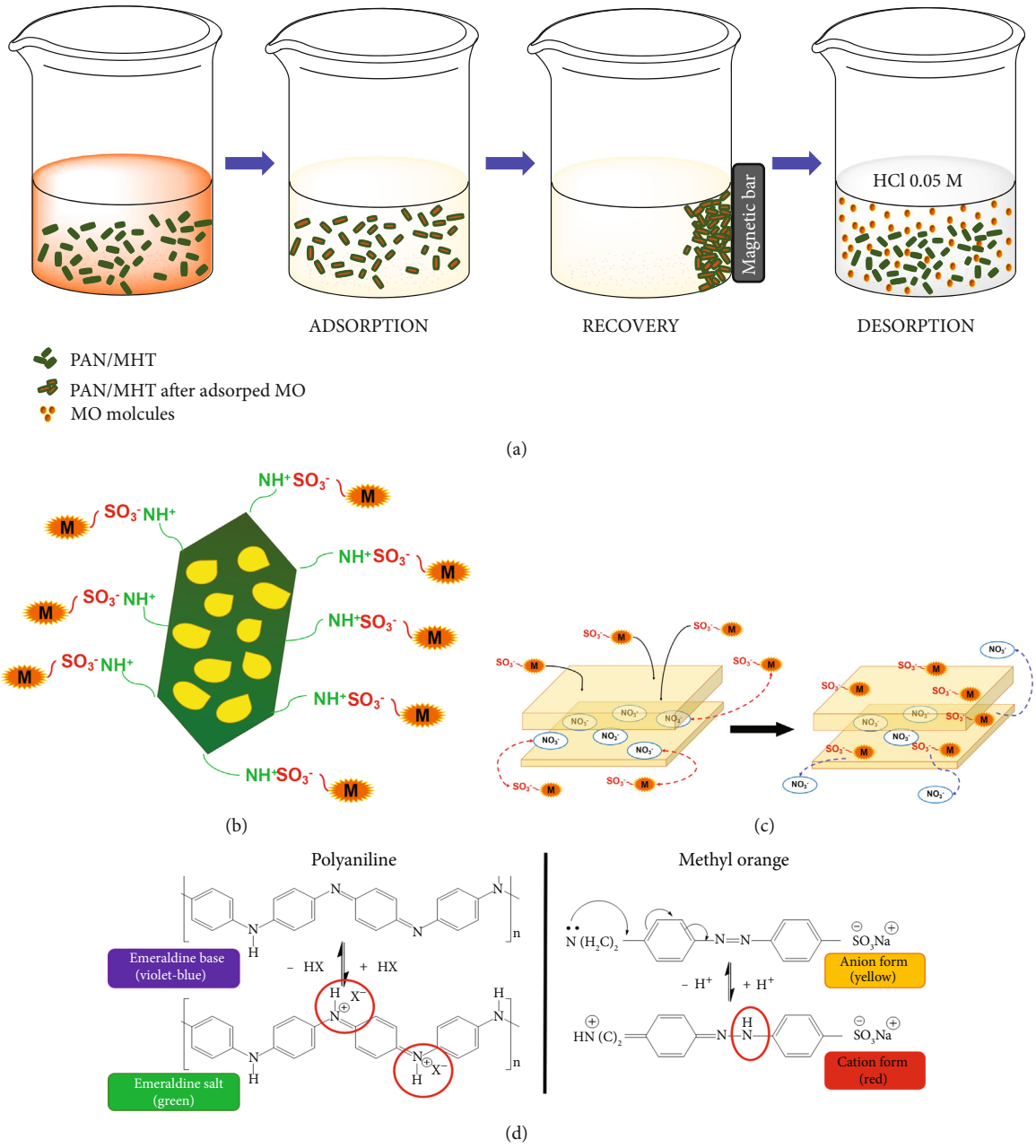

Figure 17: Schematic illustration of the adsorption and desorption mechanism of MO on Pan/MHT.

a conducting polymer with NH^+ group on full backbone that will interact with M-SO3$^-$. The electrostatic interactions are preferably involved in MO adsorption onto Pan particles. Besides, the adsorption experiment studied on Pan/MHT was found to have followed the pseudosecond-order model which indicates the chemisorption mechanism of Pan/MHT

(ii) The presence of MHT gives the good adsorption of MO because of the anion exchangeable. For this mechanism, the anion associated with the interlayer Pan/MHT is exchanged with MO anionic molecules in solution. It also means that the MO anion will be trapped into the interlayer structure, and it indicates the physical adsorption mechanical of Pan/MHT

4. Conclusion

The MHT material has been synthesized with 0.1 g Fe_3O_4 added during the coprecipitation process with the Zn^{2+}/Al^{3+} salt mixture to create a magnetic MHT material. Then, a series of Pan/MHT composites were successfully synthesized with different mass ratios of m_{Pan}/m_{MHT} = 0.5, 1, and 2. All Pan/MHT composites were characterized by analyzing methods of SEM, FT–IR, XRD, BET, and VSM and then studying for MO adsorption. The key findings of this research are

(i) 2 Pan/MHT was the best material with high surface area (15.46 m^2/g), high Hc (18.56 Oe), and low Ms (23.38×10^{-3}) and Mr (0.91×10^{-3})

(ii) According to the MO adsorption kinetic studies, all of 0.5 Pan/MHT, 1 Pan/MHT, and 2 Pan/MHT composites are suitable with pseudosecond–order model, based on the correlation coefficient ($R^2 = 0.994, 0.998$, and 0.999 corresponding to 0.5 Pan/MHT, 1 Pan/MHT, and 2 Pan/MHT), and the experimental and calculated values of Q_e are not much different. 2 Pan/MHT had the highest adsorption capacity in studying the effect of time contact and pH of MO solution

(iii) The R^2 of both Langmuir and Freundlich models of all three adsorbents is higher than 0.91; so, the adsorption of MO onto Pan/MHT composite appropriate with either monolayer of dyeing molecules covers the Pan/MHT surface or interaction between adsorbents and MO molecules

(iv) The adsorption energy of all 0.5 Pan/MHT, 1 Pan/MHT, and 2 Pan/MHT is 0.273, 0.277, and 0.269 kJ/mol, and all of them are below 8 kJ/mol. This result indicates that the adsorption process of MO on three kinds of Pan/MHT composites is physical adsorption

(v) Pan/MHT was also investigated to reuse after desorption of MO in 0.1 M HCl, and the result shows that 2 Pan/MHT can be reused for 4 cycles with $Q_e = 79.66$ mg/g

(vi) The mechanism of MO adsorption onto Pan/MHT composite is either of the surface adsorption or other types of interactions, such as electrostatic interaction, ion exchange, hydrogen bonding, and van der Waals forces

Data Availability

The data used to support the findings of this study are available from the corresponding author upon request.

Conflicts of Interest

The authors declare that there is no conflict of interest regarding the publication of this paper.

Acknowledgments

This work was supported by Kurita Water and Environment Foundation (KWEF) for the award of KURITA Overseas Research Grant 2020 under Grant [20Pvn032-K43]. The authors thank to Institute of Chemical Technology for their warmly analysis equipment support.

References

[1] Y. el maguana, N. Elhadiri, M. Bouchdoug, M. Benchanaa, and A. Boussetta, "Optimization of preparation conditions of novel adsorbent from sugar scum using response surface methodology for removal of methylene blue," *Journal of Chemistry*, vol. 2018, Article ID 2093654, 10 pages, 2018.

[2] R. Kant, "Adsorption of dye eosin from an aqueous solution on two different samples of activated carbon by static batch method," *Journal of Water Resource and Protection*, vol. 4, no. 2, pp. 93–98, 2012.

[3] U. Maheshwari, D. Deshpande, K. Zare, and P. Vardhe, "Removal of Dye from Aqueous Solution by Using Activated Carbon," *Research Journal of Engineering Science*, vol. 6, no. 7, 2017.

[4] P. K. Malik, "Dye removal from wastewater using activated carbon developed from sawdust: adsorption equilibrium and kinetics," *Journal of Hazardous Materials*, vol. 113, no. 1–3, pp. 81–88, 2004.

[5] H. O. Soonmi, "Removal of dye by adsorption onto activated carbons: review," *Eurasian Journal of Analytical Chemistry*, vol. 13, no. 4, pp. 332–338, 2018.

[6] A. A. Attia, W. E. Rashwan, and S. A. Khedr, "Capacity of activated carbon in the removal of acid dyes subsequent to its thermal treatment," *Dyes and Pigments*, vol. 69, no. 3, pp. 128–136, 2006.

[7] E. Heraldy, S. Santosa, T. Triyono, and K. Wijaya, "Anionic and Cationic Dyes Removal from Aqueous Solutions by Adsorption onto Synthetic Mg/Al Hydrotalcite-Like Compound," *Indonesian Journal of Chemistry*, vol. 15, no. 3, pp. 234–241, 2015.

[8] N. Lazaridis, T. D. Karapantsios, and D. Georgantas, "Kinetic analysis for the removal of a reactive dye from aqueous solution onto hydrotalcite by adsorption," *Water Research*, vol. 37, no. 12, pp. 3023–3033, 2003.

[9] A. El Khanchaoui, M. Sajieddine, M. Mansori, and A. Essoumhi, "Anionic dye adsorption on ZnAl hydrotalcite-type and regeneration studies based on "memory effect"," *International Journal of Environmental Analytical Chemistry*, pp. 1–19, 2020.

[10] V. T. Lam, T.-U. T. Dao, H.-T. T. Nguyen et al., "Process optimization studies of Congo red dye adsorption onto magnesium aluminium layered double hydroxide using response surface methodology," *Polish Journal of Environmental Studies*, vol. 30, no. 1, pp. 679–687, 2021.

[11] E. Erdem, G. Cölgeçen, and R. Donat, "The removal of textile dyes by diatomite earth," *Journal of Colloid and Interface Science*, vol. 282, no. 2, pp. 314–319, 2005.

[12] K. Xia, X. Liu, Z. Chen, L. Fang, H. Du, and X. Zhang, "Efficient and sustainable treatment of anionic dye wastewaters using porous cationic diatomite," *Journal of the Taiwan Institute of Chemical Engineers*, vol. 113, pp. 8–15, 2020.

[13] B. H. Dang Son, V. Quang Mai, D. Xuan du, N. Hai Phong, and D. Quang Khieu, "A study on astrazon black AFDL dye adsorption onto Vietnamese diatomite," *Journal of Chemistry*, vol. 2016, Article ID 8685437, 11 pages, 2016.

[14] R. Zheng, H. Gao, J. Guan, Z. Ren, and J. Tian, "Characteristics of cationic red X-GRL adsorption by diatomite tailings," *Journal of Wuhan University of Technology-Mater. Sci. Ed.*, vol. 32, no. 5, pp. 1038–1047, 2017.

[15] Y.-H. Zhao, J.-T. Geng, J.-C. Cai, Y.-F. Cai, and C.-Y. Cao, "Adsorption performance of basic fuchsin on alkali-activated diatomite," *Adsorption Science & Technology*, vol. 38, no. 5–6, pp. 151–167, 2020.

[16] B. Guezzen, M. Adjdir, B. Medjahed, M. A. Didi, and P. G. Weidler, "Kinetic study and box–Behnken design approach

to optimize the sorption process of toxic azo dye onto organo-modified bentonite," *Canadian Journal of Chemistry*, vol. 98, no. 5, pp. 215–221, 2020.

[17] A. Berez, F. Ayari, N. Abidi, G. Schäfer, and M. Trabelsi-Ayadi, "Adsorption-desorption processes of azo dye on natural bentonite: batch experiments and modelling," *Clay Minerals*, vol. 49, no. 5, pp. 747–763, 2014.

[18] H. Zhang, J. Zhou, Y. Muhammad et al., "Citric acid modified bentonite for Congo red adsorption," *Frontiers in Materials*, vol. 6, p. 5, 2019.

[19] S. A. S. Aldbouni, E. A. S. Alhyali, and A. A. H. Alkazraji, "Equilibrium and thermodynamic studys of adsorption of azo dyes on the local bentonite clay," *Journal of Education and Science*, vol. 28, no. 2, pp. 50–70, 2019.

[20] P. Semeraro, "Removal of an azo textile dye from wastewater by cyclodextrin-epichlorohydrin polymers," in *Cyclodextrin - A Versatile Ingredient, Ch. 13*, J. A. Gabaldón, Ed., IntechOpen, Rijeka, 2018.

[21] G. Bayramoglu and M. Y. Arica, "Grafting of regenerated cellulose films with fibrous polymer and modified into phosphate and sulfate groups: application for removal of a model azo-dye," *Colloids and Surfaces A: Physicochemical and Engineering Aspects*, vol. 614, article 126173, 2021.

[22] S. Zeng, J. Tan, X. Xu, X. Huang, and L. Zhou, "Facile synthesis of amphiphilic peach gum polysaccharide as a robust host for efficient encapsulation of methylene blue and methyl orange dyes from water," *International Journal of Biological Macromolecules*, vol. 154, pp. 974–980, 2020.

[23] Y. Song, J. Tan, G. Wang, and L. Zhou, "Superior amine-rich gel adsorbent from peach gum polysaccharide for highly efficient removal of anionic dyes," *Carbohydrate Polymers*, vol. 199, pp. 178–185, 2018.

[24] H. Gao, S. Zhao, X. Cheng, X. Wang, and L. Zheng, "Removal of anionic azo dyes from aqueous solution using magnetic polymer multi-wall carbon nanotube nanocomposite as adsorbent," *Chemical Engineering Journal*, vol. 223, pp. 84–90, 2013.

[25] X. Meng, B. Scheidemantle, M. Li et al., "Synthesis, characterization, and utilization of a lignin-based adsorbent for effective removal of azo dye from aqueous solution," *ACS Omega*, vol. 5, no. 6, pp. 2865–2877, 2020.

[26] R. C. da Silva, S. B. de Aguiar, P. L. R. da Cunha, R. C. M. de Paula, and J. P. A. Feitosa, "Effect of microwave on the synthesis of polyacrylamide-g-chitosan gel for azo dye removal," *Reactive and Functional Polymers*, vol. 148, article 104491, 2020.

[27] Y. Yildirim, H. Yilmaz, G. Ak, and S. Sanlier, "New copolymer of acrylamide with allyl methacrylate and its capacity for the removal of azo dyes," *Polímeros*, vol. 25, no. 2, pp. 137–145, 2015.

[28] M. Ait Himi, S. El Ghachtouli, A. Amarray, Z. Zaroual, P. Bonnaillie, and M. Azzi, "Removal of azo dye calcon using polyaniline films electrodeposited on SnO2 substrate," *Physical Chemistry Research*, vol. 8, no. 1, pp. 111–124, 2020.

[29] R. S. Aliabadi and N. O. Mahmoodi, "Synthesis and characterization of polypyrrole, polyaniline nanoparticles and their nanocomposite for removal of azo dyes; sunset yellow and Congo red," *Journal of Cleaner Production*, vol. 179, pp. 235–245, 2018.

[30] K. Ghosh, N. Bar, A. B. Biswas, and S. K. Das, "Removal of methylene blue (Aq) using untreated and acid-treated eucalyptus leaves and GA-ANN modelling," *The Canadian Journal of Chemical Engineering*, vol. 97, no. 11, pp. 2883–2898, 2019.

[31] I. Ghosh, S. Kar, T. Chatterjee, N. Bar, and S. Das, "Removal of methylene blue from aqueous solution using _Lathyrus sativus_ husk: adsorption study, MPR and ANN modelling," *Process Safety and Environmental Protection*, vol. 149, pp. 345–361, 2021.

[32] T. Posati, A. Listwan, G. Sotgiu, A. Torreggiani, R. Zamboni, and A. Aluigi, "Keratin/hydrotalcites hybrid sponges as promising adsorbents for cationic and anionic dyes," *Frontiers in Bioengineering and Biotechnology*, vol. 8, p. 68, 2020.

[33] L. Zheng, C. Wang, Y. Shu, X. Yan, and L. Li, "Utilization of diatomite/chitosan-Fe (III) composite for the removal of anionic azo dyes from wastewater: equilibrium, kinetics and thermodynamics," *Colloids and Surfaces A: Physicochemical and Engineering Aspects*, vol. 468, pp. 129–139, 2015.

[34] Y. Z. Zhang, J. Li, W. J. Li, and Y. Li, "Adsorption of sunset yellow FCF from aqueous solution by chitosan-modified diatomite," *Water Science and Technology*, vol. 72, no. 10, pp. 1861–1868, 2015.

[35] X.-J. Wu, J.-D. Wang, and L.-Q. Cao, "Characterization and Adsorption Performance of Chitosan/Diatomite Membranes for Orange G Removal," *e-Polymers*, vol. 16, no. 2, pp. 99–109, 2016.

[36] A. A. Khodabandelou, R. Darvishi Cheshmeh Soltani, H. Gudini, M. J. Tarrahi, and F. Fazelinia, "Removal of azo dye from synthetic wastewater using immobilized nano-diatomite within calcium alginate TT - حذف رنگ آزو از فاضلاب مصنوعی با استفاده از نانو-دیاتومیت تثبیت شده در آلژینات کلسیم," *SSUJ*, vol. 14, no. 6, pp. 17–35, 2016.

[37] Q. Liu, B. Yang, L. Zhang, and R. Huang, "Adsorption of an anionic azo dye by cross-linked chitosan/bentonite composite," *International Journal of Biological Macromolecules*, vol. 72, pp. 1129–1135, 2015.

[38] J. Tie, X. Fang, X. Wang et al., "Adsorptive removal of a reactive azo dye using polyaniline-intercalated bentonite," *Polish Journal of Environmental Studies*, vol. 26, no. 3, pp. 1259–1268, 2017.

[39] A. Sienkiewicz, A. Kierys, and J. Goworek, "Polymer-hybrid silica composite for the azo dye removal from aqueous solution," *Journal of Dispersion Science and Technology*, vol. 40, no. 10, pp. 1396–1404, 2019.

[40] K. Abdellaoui, I. Pavlovic, and C. Barriga, "Nanohybrid layered double hydroxides used to remove several dyes from water," *ChemEngineering*, vol. 3, no. 2, p. 41, 2019.

[41] H. Zaghouane-Boudiaf, M. Boutahala, and L. Arab, "Removal of methyl orange from aqueous solution by uncalcined and calcined MgNiAl layered double hydroxides (LDHs)," *Chemical Engineering Journal*, vol. 187, pp. 142–149, 2012.

[42] R. Extremera, I. Pavlovic, M. R. Pérez, and C. Barriga, "Removal of acid orange 10 by calcined mg/Al layered double hydroxides from water and recovery of the adsorbed dye," *Chemical Engineering Journal*, vol. 213, pp. 392–400, 2012.

[43] C. Prasad, H. Tang, and W. Liu, "Magnetic Fe3O4 based layered double hydroxides (LDHs) nanocomposites (Fe3O4/LDHs): recent review of progress in synthesis, properties and applications," *Journal of Nanostructure in Chemistry*, vol. 8, no. 4, pp. 393–412, 2018.

[44] M. Duhan and R. Kaur, "Adsorptive removal of methyl Orange with polyaniline nanofibers: an unconventional

adsorbent for water treatment," *Environmental Technology*, vol. 41, no. 23, pp. 2977–2990, 2020.

[45] M. Tanzifi, M. Tavakkoli Yaraki, M. Karami et al., "Modelling of dye adsorption from aqueous solution on polyaniline/carboxymethyl cellulose/TiO_2 nanocomposites," *Journal of Colloid and Interface Science*, vol. 519, pp. 154–173, 2018.

[46] M. Bhaumik, R. I. McCrindle, A. Maity, S. Agarwal, and V. Gupta, "Polyaniline nanofibers as highly effective reusable adsorbent for removal of reactive black 5 from aqueous solutions," *Journal of Colloid and Interface Science*, vol. 466, pp. 442–451, 2016.

[47] M. Saad, H. Tahir, J. Khan, U. Hameed, and A. Saud, "Synthesis of polyaniline nanoparticles and their application for the removal of crystal violet dye by ultrasonicated adsorption process based on response surface methodology," *Ultrasonics Sonochemistry*, vol. 34, pp. 600–608, 2017.

[48] A. Muhammad, A.-H. Shah, and S. Bilal, "Comparative study of the adsorption of acid blue 40 on polyaniline, magnetic oxide and their composites: synthesis, characterization and application," *Materials*, vol. 12, no. 18, p. 2854, 2019.

[49] M. Ayad and A. A. el-Nasr, "Adsorption of cationic dye (methylene blue) from water using polyaniline nanotubes base," *The Journal of Physical Chemistry C*, vol. 114, no. 34, pp. 14377–14383, 2010.

[50] M. Ayad and A. A. el-Nasr, "Anionic dye (acid green 25) adsorption from water by using polyaniline nanotubes salt/silica composite," *Journal of Nanostructure in Chemistry*, vol. 3, no. 1, 2012.

[51] V. Sharma, P. Rekha, and P. Mohanty, "Nanoporous hypercrosslinked polyaniline: an efficient adsorbent for the adsorptive removal of cationic and anionic dyes," *Journal of Molecular Liquid*, vol. 222, pp. 1091–1100, 2016.

[52] T. Sulistyaningsih, S. J. Santosa, D. Siswanta, and B. Rusdiarso, "Preparation of magnetite-mg/Al hydrotalcite through hydrothermal process and subsequent calcination," *Advanced Materials Research*, vol. 1101, pp. 336–339, 2015.

[53] K. Zhu, Y. Gao, X. Tan, and C. Chen, "Polyaniline modified mg/Al layered double hydroxide composites and their application in efficient removal of Cr (VI)," *ACS Sustainable Chemistry & Engineering*, vol. 4, no. 8, pp. 4361–4369, 2016.

[54] X. Wu, X. Tan, S. Yang et al., "Coexistence of adsorption and coagulation processes of both arsenate and NOM from contaminated groundwater by nanocrystallined mg/Al layered double hydroxides," *Water Research*, vol. 47, no. 12, pp. 4159–4168, 2013.

[55] T. Wen, Q. Fan, X. Tan et al., "A Core-shell structure of polyaniline coated protonic titanate nanobelt composites for both Cr(VI) and humic acid removal," *Polymer Chemistry*, vol. 7, no. 4, pp. 785–794, 2016.

[56] S. S. Umare, B. H. Shambharkar, and R. S. Ningthoujam, "Synthesis and characterization of polyaniline- Fe_3O_4 nanocomposite: electrical conductivity, magnetic, electrochemical studies," *Synthetic Metals*, vol. 160, no. 17-18, pp. 1815–1821, 2010.

[57] M. Jokar, R. Foroutani, M. Safaralizadeh, and K. Farhadi, "Synthesis and characterization of polyaniline/Fe_3O_4 magnetic nanocomposite as practical approach for fluoride removal process," *Annual Research & Review in Biology*, vol. 4, no. 21, pp. 3262–3273, 2014.

[58] M. Duhan and R. Kaur, "Nano-structured polyaniline as a potential adsorbent for methylene blue dye removal from effluent," *Journal of Composites Science*, vol. 5, no. 1, p. 7, 2021.

[59] N. Wang, J. Chen, J. Wang, J. Feng, and W. Yan, "Removal of methylene blue by polyaniline/TiO_2 hydrate: adsorption kinetic, isotherm and mechanism studies," *Powder Technology*, vol. 347, pp. 93–102, 2019.

[60] A. I. Okoye, P. M. Ejikeme, and O. D. Onukwuli, "Lead removal from wastewater using fluted pumpkin seed Shell activated carbon: adsorption modeling and kinetics," *International Journal of Environmental Science & Technology*, vol. 7, no. 4, pp. 793–800, 2010.

[61] I. Langmuir, "The constitution and fundamental properties of solids and liquids. PART I. SOLIDS," *Journal of the American Chemical Society*, vol. 38, no. 11, pp. 2221–2295, 1916.

[62] H. Freundlich, "Über Die Adsorption in Lösungen," *Zeitschrift für Physikalische Chemie*, vol. 57U, no. 1, pp. 385–470, 1907.

[63] M. Dubinin, "The equation of the characteristic curve of activated charcoal," *Proceedings of the USSR Academy of Sciences*, vol. 55, pp. 327–329, 1947.

[64] A. Günay, E. Arslankaya, and I. Tosun, "Lead removal from aqueous solution by natural and pretreated clinoptilolite: adsorption equilibrium and kinetics," *Journal of Hazardous Materials*, vol. 146, no. 1–2, pp. 362–371, 2007.

[65] H. PS, L. Joseph, and D. A, "Photocatalytic degradation of textile dyes by hydrogel supported titanium dioxide nanoparticles," *Journal of Environmental Engineering and Ecological Science*, vol. 2, no. 1, p. 2, 2013.

[66] K. Haitham, S. Razak, and M. A. Nawi, "Kinetics and isotherm studies of methyl orange adsorption by a highly recyclable immobilized polyaniline on a glass plate," *Arabian Journal of Chemistry*, vol. 12, no. 7, pp. 1595–1606, 2019.

[67] L. S. Mendieta-Rodríguez, L. M. González-Rodríguez, J. J. Alcaraz-Espinoza, A. E. Chávez-Guajardo, and J. C. Medina-Llamas, "Synthesis and characterization of a polyurethane-polyaniline macroporous foam material for methyl orange removal in aqueous media," *Materials Today Communications*, vol. 26, article 102155, 2021.